

Andreas Christen^{(1)*}, Roland Vogt⁽¹⁾⁽¹⁾ University of Basel, Institute of Meteorology, Climatology and Remote Sensing, Basel, Switzerland.

1 INTRODUCTION

Flow within plant canopies is strongly influenced by individual roughness elements, with the consequence that turbulence statistics and flux densities are vertically and horizontally inhomogeneous. In contrast, most models treat exchange processes one-dimensional and rely on horizontally (spatially) averaged variables. By averaging over time and space, contributions that result from local inhomogeneities in the mean flow have to be taken into account. These dispersive fluxes result from spatial correlations of the local average departure from the spatial-temporal mean (Raupach and Shaw, 1982).

Often, dispersive fluxes are considered irrelevant and are neglected. It is important to know at least an approximation of their order of magnitude to quantify associated errors of this simplification.

Wind tunnel results suggest that dispersive fluxes are insignificant above and in the upper part of the canopies (Raupach *et al.*, 1986). Recently, two physical scale model studies investigated dispersive fluxes in the bottom layers of model canopies. It was found, that there they can have the same magnitude as the turbulent fluxes (Böhm *et al.*, 2000). Poggi *et al.* (2004) concluded that dispersive fluxes are only important in sparse canopies. Up to now, no experimental results are available from real canopies.

2 EXPERIMENTAL SETUP

To estimate the magnitude of dispersive fluxes of momentum and sensible heat in a real canopy, 8 ultrasonic anemometer-thermometers were deployed in an irregular array of 70 by 70 m within a sparse cork oak plantation (Fig. 1). The cork oak plantation is located in flat terrain near Rio Frio, Portugal (38°38'15" Lat, -08°50'48" Lon). It has a density of 76 trees ha⁻¹ and a mean height h of 10 m. A patchy understorey (*Cystus crispus*) reaches 0.4 m on average.

One Gill R2 (C1) and seven Campbell Scientific Instrument CSAT3 ultrasonic anemometer-thermometers (C2-C8) were mounted in the trunk space on small masts (Fig. 2). The instruments were installed at a uniform height of 1.8 m ($z/h \sim 0.18$). They were carefully leveled, and oriented into the prevailing wind

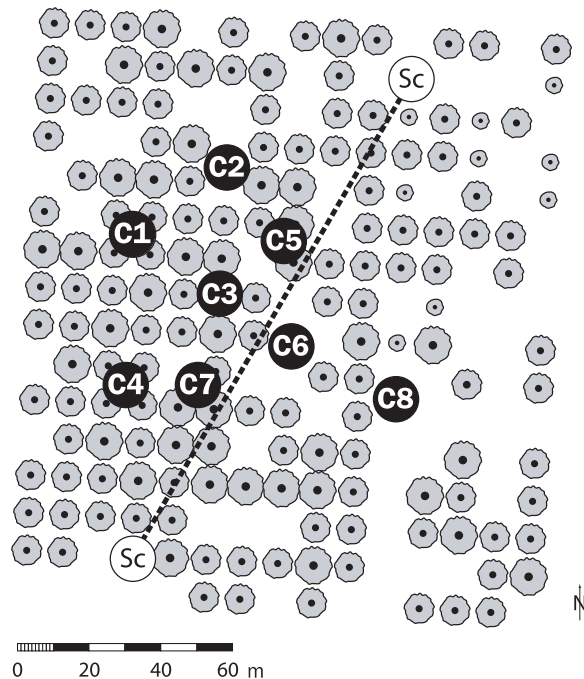


Fig. 1: Map of a subset of the cork oak plantation illustrating the experimental layout. C1 to C8 refer to the canopy ultrasonic anemometer-thermometers. Sc denotes the path of a small aperture scintillometer (see Vogt *et al.*, 2004, *this conference* for details). Site C8 consists of a 20m tower with simultaneous ultrasonic anemometer measurements at tower top.



Fig. 2: One of the eight (identical) 1.8 m masts in the trunk space equipped with a Campbell Scientific CSI CSAT 3. The photo shows position C5.

* Corresponding author address:

Andreas Christen
Institute of Meteorology, Climatology and Remote Sensing,
Department of Geosciences, University of Basel
Klingelbergstrasse 27, CH-4056 Basel, Switzerland
e-mail: andreas.christen@unibas.ch

direction (NW). This setup covers the vertical region where substantial dispersive fluxes are suggested by the wind tunnel studies.

Analysis was done for a summertime three day period (July 10 to 12 2003). The meteorological forcing during these days was dominated by a wind system, with moderate daytime winds from NNW up to 4 m/s (10 m above the canopy) and dominantly clear sky (some clouds at 07/12). Nights were characterized by lower wind speeds of 1.5 m/s from same direction.

3 DATA PROCESSING

Raw data from the ultrasonic anemometer-thermometers were sampled at 20 Hz and synchronized on one system. Block averages over 30 min were deduced without detrending. For each run, the coordinate system was rotated by a single rotation around the vertical axis into the mean wind direction above the canopy. The direction above the canopy was derived from an additional ultrasonic anemometer-thermometer mounted at twice the canopy height (Position C8, 20 m tower). Average dispersive fluxes (denoted by double primes) were calculated using (1), where j is the instrument index (and the total number of instruments is $J=8$). Angular brackets denote spatial averages over all eight canopy positions.

$$\langle \bar{u}'' \bar{w}'' \rangle = \frac{1}{J} \sum_{j=1}^J (\bar{u}_j - \langle \bar{u} \rangle) (\bar{w}_j - \langle \bar{w} \rangle) \quad (1)$$

The same procedure is applied to vertical wind w and virtual temperature θ .

4 RESULTS

First, we have to test, if the whole setup can sample the processes of interest. It is obvious, that the horizontal domain of the experiment limits results to dispersive fluxes that are present in scales smaller than half the size of the experimental array x , i.e. the dispersive Eulerian length scale of both wind components $\Lambda_{u''}$ and $\Lambda_{w''}$, and virtual temperature $\Lambda_{\theta''}$ must be all significantly lower than $x/2$ (35m). The dispersive Eulerian length scales cannot be determined with the current setup, however, the individual trees of the plantation are supposed to be the primary source of the local deviations from the spatial-temporal mean (for both, momentum and temperature). Their highest spectral density is the scale of the canopy height which is equal to the horizontal separation of the trees ($h=d=10m$). This roughly suggests that the setup is adequate because $h=d < x/2$.

4.1 Overall magnitude of the dispersive momentum flux

The temporal variations of the spatially averaged turbulent and dispersive momentum fluxes are shown in Fig. 3. During daytime, when wind speeds are higher and stratification is unstable, not only turbulent fluxes are measured, but also a dispersive flux term results, which is consistently present on all 3 days.

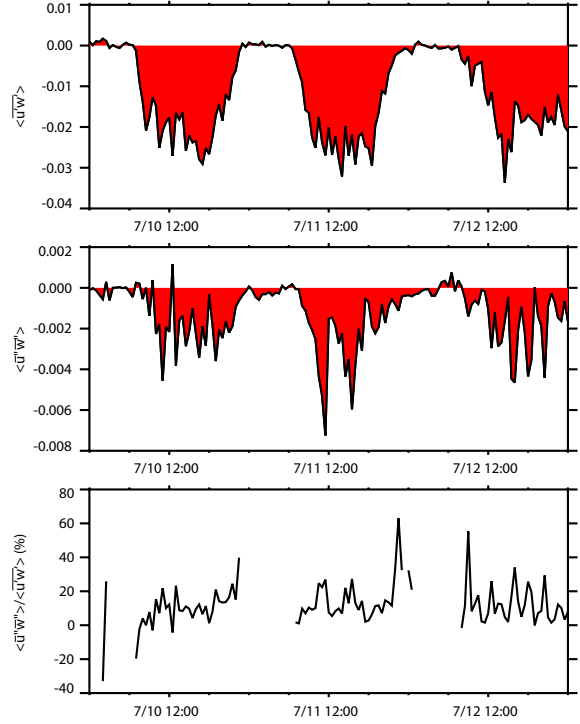


Fig. 3: Time series over three days of the spatially averaged turbulent flux of momentum (top), the spatially averaged dispersive flux (middle) and the ratio between turbulent and dispersive flux of momentum (bottom). Ratios where the turbulent flux is below $10^{-3} m^2/s^2$ are not drawn as ratio, which applies for most night situations. Times are indicated in LST.

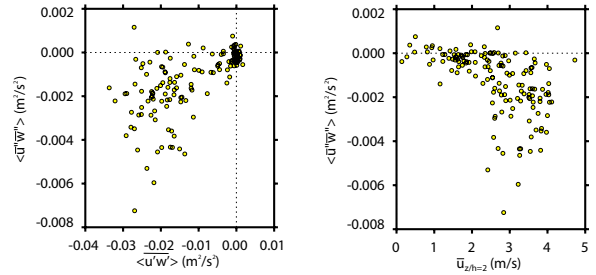


Fig. 4: Dispersive fluxes of momentum as function of turbulent flux (left) and mean wind speed above the canopy (right) with all situations from 7/10 to 7/12 included.

Roughly it can be seen, that the stronger the turbulent flux, the stronger the dispersive flux (Fig. 4, left). The magnitude of the ratio dispersive to turbulent flux of momentum is typically on the order of 0-20% (on average 14%). This can be attributed to the increased magnitude of the spatial mean wind deviations \bar{u}'' and \bar{w}'' , with increasing mean wind speed (Fig. 4, right). The results support the wind tunnel findings and show that dispersive fluxes of momentum exist and are measurable in the lower canopy, even if their relative importance is not outstanding.

Tab. 1: Local characteristics of the dispersive and turbulent momentum flux for all positions of the array. Statistics are only calculated from situations where all instruments provide valid data, and have a measured wind speed above the canopy which is > 2 m/s, and a wind direction in the range $280^\circ - 360^\circ$. The spatial average of the $u'w'$ covariance must be below -0.001 ($n=68/144$). Shown are median values. "Quadr." refers to the vector mean position in the quadrant plot (Fig. 5).

	Dispersive Flux			Turbulent Flux	
	P_j^n	$(\overline{u''w''})_j / (\overline{u''w''})_j$	Quadr.	$(\overline{u''w''})_j / \langle \overline{u''w''} \rangle$	r_{uw}
C1	+0.03	+0.03	2	0.92	-0.55
C2	+0.01	+0.00	4	1.47	-0.77
C3	+0.20	+0.17	2	0.92	-0.88
C4	+0.03	+0.01	4	1.09	-0.88
C5	+0.00	+0.05	3	0.06	-0.03
C6	+0.22	+0.12	2	1.57	-0.49
C7	+0.52	+0.26	4	1.66	-0.56
C8	-0.04	-0.04	1	0.36	-0.11

4.2 Effect of single array positions

Due to the low number of spatial samples, results are very sensitive to local effects. The eight instrument positions C1 to C8 must representatively describe the spatial heterogeneity. One problem can be excluded: An inappropriate leveling of the instruments would result in a counterbalancing of positive and negative (artificial) dispersive flux contributions and would not lead to the consistent pattern of a negative correlation between $\overline{u''}$ and $\overline{w''}$ for the majority of the instruments. Therefore, the observed dispersive flux is not an artifact of a wrong instrument leveling.

In order to verify the effects of single instrument positions, for each position and time step a dispersive stress fraction P_j^n has been calculated according formula (2). P_j^n explains the dispersive stress contribution from an individual sampling position to the overall dispersive flux:

$$P_j^n = \frac{1}{J} \frac{(\overline{u''w''})_j}{\langle \overline{u''w''} \rangle} \quad (2)$$

The majority of the sampling positions show positive dispersive stress fractions P_j^n (Tab. 1). Dispersive stress fractions are inhomogeneous distributed in space. For example, position C7 explains over 50% of the total dispersive momentum flux, and 2 other positions fill roughly the remaining part (C3, C6). At 7 of the 8 positions, the dispersive flux transports momentum in the same direction as the temporally and spatially averaged turbulent flux does.

One instrument contributes with a negative stress fraction (C8), which means that this position is characterized by a (globally) counter gradient dispersive flux. Interestingly, positions with a P_j^n close to zero or a negative P_j^n show low turbulent fluxes and low turbulent correlation coefficients r_{uw} . This suggests that these instruments are located in inefficient regimes. Position C8 for example is located upwind of a large open area (Fig. 1) during the investigated NW wind. Here a dynamical low-level acceleration behind the trees surely modifies the flow.

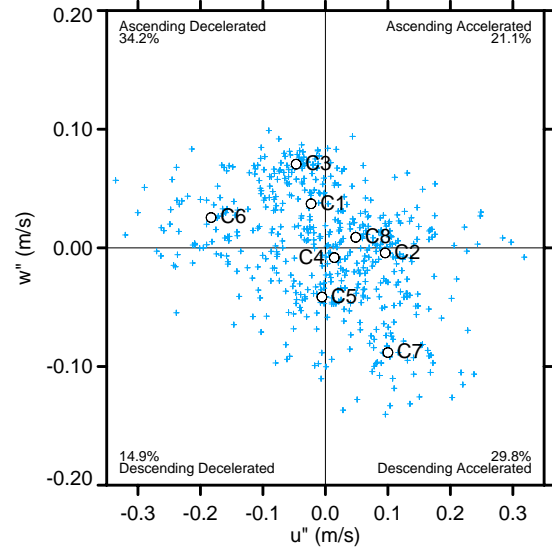


Fig. 5: Ensemble quadrant plot of dispersive terms of longitudinal and vertical wind from 68 runs. Data cover the same conditions as selected for Tab. 1. The (vector) average position of each instrument position is drawn with a circle. Numbers in the corners are the percentage of spatial locations in the particular quadrant, denoted as "area fractions" (see Eq. 5).

4.3 Quadrant analysis of dispersive fluxes

In analogy to the classical quadrant analysis which investigates time series and classifies instantaneous values into outward interactions, ejections, sweeps, inward interactions and bursts (Lu and Willmarth, 1973), the method of quadrant analysis can be also applied to dispersive terms, where the location of an instrument position in a quadrant plot describes the mean flow characteristics of that particular location in space. Instead of $u'(t)$ and $w'(t)$ we draw $\overline{u''}(j)$ and $\overline{w''}(j)$ of a run, resulting in ascending accelerated zones (Q1), ascending decelerated zones (Q2), descending decelerated zones (Q3) and descending accelerated zones (Q4). For each of the quadrants, a dispersive stress fraction S_q^n can be calculated, which describes the dispersive stress contribution from a single quadrant:

$$S_q^n = \frac{[\overline{u''w''}]_q}{\langle \overline{u''w''} \rangle} \quad (3)$$

Where the squared brackets denote a conditional average from one of the quadrants with

$$[\overline{u''w''}]_q = \frac{1}{J} \sum_{j=1}^J \overline{u''w''}_j I_j \quad (4)$$

I_j is an indicator function with is equal 1 if the actual position (instrument) j is in quadrant q , and 0 otherwise. It follows from Equations (3) and (4) that

$$\sum_{q=1}^4 S_q^n = 1 \quad (5)$$

For a single run only $J = 8$ data points can be analyzed, which is a very small number to perform an analysis. However, the steady wind speed and direction allows calculating an ensemble over several nearly identical runs, which helps to retain a larger number of samples (Fig. 5).

On average, all instruments except C5 and C8 (where zero or a negative stress fraction is measured) find place in quadrants 2 and 4, which indicates that either lower horizontal wind speeds are measured together with mean upwind or higher horizontal wind speeds are present if a mean downward motion is dominating the flow.

If we assume the instruments to be a representative spatial sample, i.e. each instrument represents 1/8 of the total area, the percentage of locations in a particular quadrant in Fig. 5 can be interpreted as "area fractions" (in analogy to "time fractions" in the turbulent quadrant analysis):

$$A_q'' = \frac{1}{J} \sum_{j=1}^J I_j \quad (6)$$

The results point out, that 64% of the area (in the 1.8 m height layer) contributes to negative dispersive fractions (Q2 and 4), and 36% are dominated by dispersive 'counter-gradient' regimes (Q1 and 3). Finally, the measure $\Delta S''_{Q4-S''_{Q2}}$ can be used to determine the relative importance of ascending decelerated zones (Q2) to descending accelerated zones (Q4). Only in 38% of all runs $\Delta S''_{Q4-S''_{Q2}}$ is negative. Ascending decelerated zones are less important. The majority (62%) of all runs show a dominance of descending accelerated zones that contribute to the dispersive flux. This may reflect the fact that the above canopy flow is more structured and downward motions reflect the properties (momentum) of the overall wind profile, while upward motions have higher entropy due to the local effects of canopy elements.

However, the influence of one single instrument (C7) is very dominant, and therefore these detailed results should not be considered to be of general significance. Surely, further experiments are needed.

4.4 Dispersive flux of sensible heat

The dispersive flux of sensible heat is much lower, typically in the range between -5 and +5% of the turbulent flux and -1% on average (Fig. 6). In the morning of all three days, the spatially averaged dispersive flux points in the same direction as the turbulent flux. During afternoon however, the turbulent flux and the dispersive flux show opposite signs. This can be an effect of the changing relative sun position and shadows on the instruments, and finally an effect of a single instrument. Since acoustic temperature measurements are very sensitive to path length, the instrument with only one path for temperature measurement (Gill R2, C1) has been excluded from analysis. Further, instrumental temperature offsets have been adjusted by comparing the instruments during a night condition where temperature was supposed to

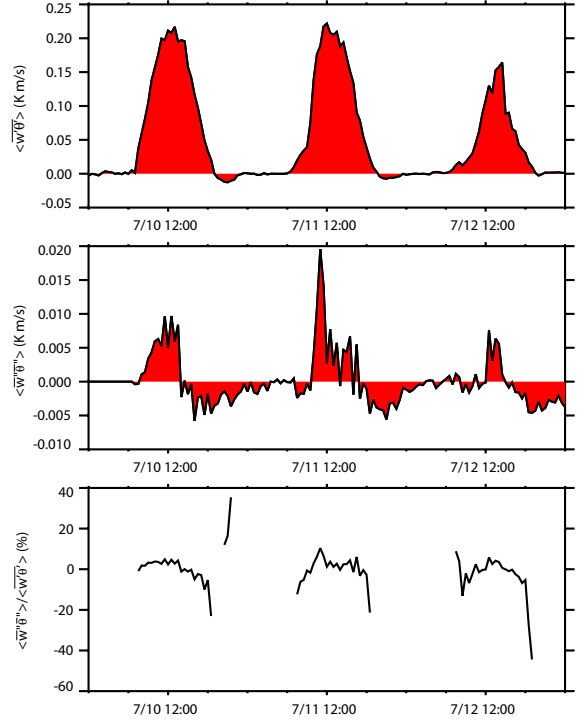


Fig. 6: Similar to Fig. 3, time series over the three days of the spatially averaged kinematic turbulent flux of sensible heat (top), the corresponding spatially averaged dispersive flux (middle) and the ratio between turbulent and dispersive flux (bottom).

Tab. 2: Instrument specific flux fractions for vertical dispersive flux of sensible heat, and relative ratio dispersive to turbulent flux for each position separately.

Position	F_j'' $w''t'' > 0$	F_j'' $w''t'' < 0$	$(\overline{w''\theta''})_j / (\overline{w''\theta''})_j$
C2	+0.02	+0.02	-0.01
C3	-0.03	+0.47	-0.03
C4	+0.04	+0.01	+0.00
C5	+0.27	-0.15	+0.03
C6	+0.80	-0.07	+0.07
C7	-0.46	+0.90	-0.07
C8	+0.01	-0.04	+0.00

be uniform. Calculations were done with adjusted and uncorrected temperatures separately, but no significant difference in the magnitude of the dispersive fluxes is found. In both cases the ratio dispersive flux to turbulent flux of sensible heat is close to zero on average.

In order to verify the results, analogous to (2), dispersive flux fractions can be deduced for each instrument position (7), which are separately listed for morning hours ($\langle \overline{w''\theta''} \rangle > 0$) and afternoon situations ($\langle \overline{w''\theta''} \rangle < 0$) in Tab. 2.

$$F_j'' = \frac{1}{N} \frac{(\overline{w''\theta''})_j}{\langle \overline{w''\theta''} \rangle} \quad (7)$$

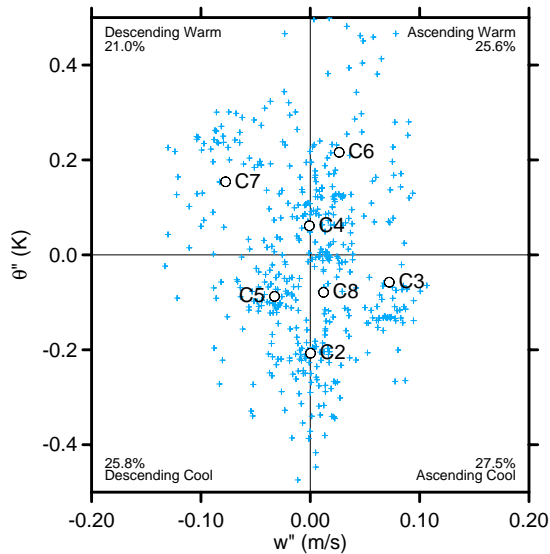


Fig. 7: Similar to Fig. 5 for dispersive terms of vertical wind and virtual temperature.

The dispersive flux fractions F_j^d suggest that the estimation of the dispersive sensible heat flux is less accurate and a high scatter between the instruments exists. All four quadrants show a very similar area fraction between 21 and 28% (Fig 7). The small observed flux densities are often an effect of single instruments, and no systematic dispersive correlation is found in contrast to the momentum flux. The instruments show low run-to-run variability in $\bar{\theta}''$, suggesting that instrumental offsets in acoustic temperature are disturbing the analysis. The present measurements show that the dispersive flux of sensible heat is negligible small on average, compared to the turbulent flux.

4.5 Closing remarks

The different importance of the two measured dispersive fluxes (momentum: 15%, sensible heat: 0% of the turbulent fluxes) can be explained by the different forcing. While the two mean wind components u and w are forced by the same mean pressure and drag field, mean temperature has a different origin, i.e. spatial distribution of roughness elements and the pattern of sunlit shadowed areas do not coincide in space. Moreover, turbulence analysis shows that typical length scales of longitudinal velocity fluctuations are significantly larger than the length scales of temperature, suggesting that horizontal wind velocity fluctuations are associated with larger structures than temperature fluctuations in the canopy.

ACKNOWLEDGEMENTS

Many thanks go to Florian Imbery (Univ. of Freiburg, Germany), Irene Lehner (Univ. of Basel, Switzerland) and Andrea Pitacco (Univ. of Padova, Italy).

REFERENCES

- Additional photos and experiment documentation:
<http://www.unibas.ch/geo/mcr/Projects/WATERUSE/>
- Böhm M, Finnigan JJ, Raupach MR (2000): 'Dispersive fluxes and canopy flows: just how important are they?'. *24th Conference on Agricultural and Forest Meteorology*, 14-18 August 2000, Davis, CA.
- Lu SS, Wilmarth WW (1973): 'Measurements of the structure of the Reynolds stress in a turbulent boundary layer'. *J. Fluid. Mech.* 60. 481-571.
- Poggi D, Katul GG, Albertson JD (2004): 'A note on the contribution of dispersive fluxes to momentum transfer within canopies', *Bound.-Layer Meteorol.* 111: 615-621.
- Raupach MR, Shaw RH (1982): 'Averaging procedures for flow within vegetation canopies', *Bound.-Layer Meteorol.* 22: 79-90.
- Raupach MR, Coppin PA, Legg BJ (1986) 'Experiments on scalar dispersion within a model plant canopy. Part I: the turbulence structure'. *Bound.-Layer Meteorol.* 35. 21-52.
- Vogt R, Christen A, Pitacco A (2003): 'Scintillometer measurements inside two tree canopies'. *This conference*, P1.26